JOURNAL OF Materials CHEMISTRY

Formation of highly ordered mesoporous silica materials adopting lyotropic liquid crystal mesophases

S. A. El-Safty*[a] and J. Evans[b]

[a]*Chemistry Department, Faculty of Science, Tanta University, Tanta, Egypt. E-mail: saes@dec1.tanta.eun.eg*
[b]*Department of Chemistry, University of Southampton, Southampton SO17 1BJ, UK*

Received 10th July 2001, Accepted 7th October 2001
First published as an Advance Article on the web 15th November 2001

Mesoporous silica materials have been synthesised in strongly acidic media at pH = 1.3 using high concentrations of a non-ionic surfactant (Brij 76) as a structure-directing agent. Well-defined ordered mesoporous silicas with hexagonal (H_I), lamellar (L_∞) and solid phase (S) structure have been prepared at room temperature according to the lyotropic liquid crystalline mesophases of Brij 76. At high temperature (60 °C), highly ordered cubic (*Ia3d*), cubic (*Im3m*) and 3-d hexagonal ($p6_3/mmc$) nanostructured materials have been produced. The synthesised materials were studied by powder X-ray diffraction (XRD), the Brunauer–Emmett–Teller (BET) method for nitrogen adsorption/desorption isotherms and surface area measurements. Transmission electron microscopy (TEM), XRD and TEM patterns for all materials show well-defined long-range porous architectures. It was found that BET surface area values of the nanostructured materials are reduced upon increasing the temperature of synthesis.

Introdution

Mesoporous silica materials are generally prepared by using surfactants as a templating agents. The synthesis can be considered in terms of a self-assembly process involving electrostatic interactions between the inorganic ions in solution and charged surfactant head groups.[1–5] Hydrogen bonding interactions between the neutral primary amine micelles and neutral inorganic species are also significant in the generation of mesoporous molecular sieves.[6,7]

The dilute surfactant solutions used in the formation of ordered, mesoporous silica, such as M41-S,[1,2] FSM-16,[5] and HMS,[6,7] limit the ability to predict the topology of the mesophases. Also only powders of micrometer dimensions (1–2 μm) are produced. The three architectures found for the M41S family of mesoporous silicas, a hexagonal phase referred to as MCM-41, a cubic phase (*Ia3d*) known as MCM-48, and MCM-50, an unstable lamellar phase, have been reported elsewhere.[8–11] In addition, cubic (*pm3n*) high quality mesoporous molecular sieves designated SBA-1 have been reported.[3–5,12] Generally, the structure of the resulting mesoporous solid is affected by the reaction conditions. Changing the pH of the medium leads to the transformation of the lamellar phase of silica to the hexagonal phase.[13] Other factors such as temperature and surfactant concentration have been observed to affect the structure formed.[14–16]

High concentrations of non-ionic surfactants have been employed for the synthesis of large uniform nanoporous monolithic silicates. In such systems lyotropic liquid crystalline phases are exploited as templates to produce long-range ordered mesoporous silicates, which are independent of the structures and charge of the amphiphiles, as shown by Attard *et al.*[17,18] The synthesis of hexagonal (H_I-silica), cubic (*Ia3d*-silica) and lamellar (L_∞-silica) silica as well as H_I-aluminium silicates have also been reported.[19]

Our approach uses high concentrations of the non-ionic surfactant Brij 76 as a template structure-directing agent to form well-defined long range ordered mesoporous silica materials. Nanoporous monolithic silicates including hexagonal (H_I), lamellar (L_∞), solid phase (S), cubic (*Ia3d*), cubic (*Im3m*), and 3-d hexagonal ($p6_3/mmc$) materials are synthesised *via* the lyotropic liquid crystal phase of the template and at different temperatures. The high quality materials synthesised are investigated by using XRD, TEM, and BET for N_2 adsorption/desorption isotherms and surface area measurements.

Experimental

Materials

Tetramethylorthosilicate (TMOS) was obtained from Fluka. Brij 76 (polyethylene (10) stearyl ether) was supplied by Sigma–Aldrich Ltd. UK.

Synthesis

In all cases of syntheses of the mesoporous silica mesophases the surfactant (Brij 76) and TMOS were mixed with agitation until homogeneous. Hydrochloric acid (diluted to pH = 1.3 with deionized water) was added quickly which led to exothermic hydrolysis. The mixture was placed under gentle vacuum until it changed from a viscous liquid to a gel-like material. As-synthesized materials were collected and allowed to stand in a sealed container at 40 °C for 20 h. For room-temperature syntheses the weight ratio of surfactant : TMOS : HCl was 1 : 2 : 1 for H_I-SiO_2,[20] 1.5 : 2 : 1 for L_∞-SiO_2, and 1.3 : 1.5 : 1 for S-SiO_2. For syntheses conducted at 60 °C, the weight ratio was 1.4 : 2 : 1 for *Ia3d*-SiO_2, 1.52 : 2 : 1 for *Im3m*-SiO_2, and 1.62 : 2 : 1 for 3-d (H_I-SiO_2). The surfactant was removed by calcination at 450 °C (3 h under nitrogen and 14 h under oxygen) for all the silica mesophase materials.

Analyses

Powder X-ray diffraction (XRD) patterns were recorded on a Siemens (θ–2θ) D5000 diffractometer with monochromated Cu-Kα radiation. Nitrogen adsorption/desorption isotherms and surface area measurements were determined following the BET method at 77 K, the data being collected with a

DOI: 10.1039/b106077p

Micromeritrics GEMINI III 2375 surface area analyzer. Transmission electron microscopy (TEM) images were recorded on a JEOL FX 2000 instrument operating at an acceleration voltage of 200 kV.

Results and discussion

The isotropic liquid produced during the hydrolysis of TMOS in the Brij 76/HCl mixture was due to the formation of methanol. The presence of the methanol in the mixture destroys the mesophase structure but removal of the methanol under vacuum allowed the mesophases to form. The generation of the monolithic material under highly acidic conditions (pH = 1.3) leads to a rapid poly-condensation process without loss of the long-range order of the mesoporous materials.[20,21]

The high concentration of Brij 76 permits the pre-existence of lyotropic liquid crystalline phases and directs the formation of monolithic nanostructured materials with different mesophases through a liquid crystal template mechanism.[8,9,20] The temperature and the surfactant concentration mainly affect the phases formed,[22] rather the structure and charge density of the surfactant.[23]

Nitrogen adsorption/desorption isotherms

N_2 adsorption/desorption isotherms for the calcined mesoporous materials are shown in Figs. 1 and 2. All the mesoporous

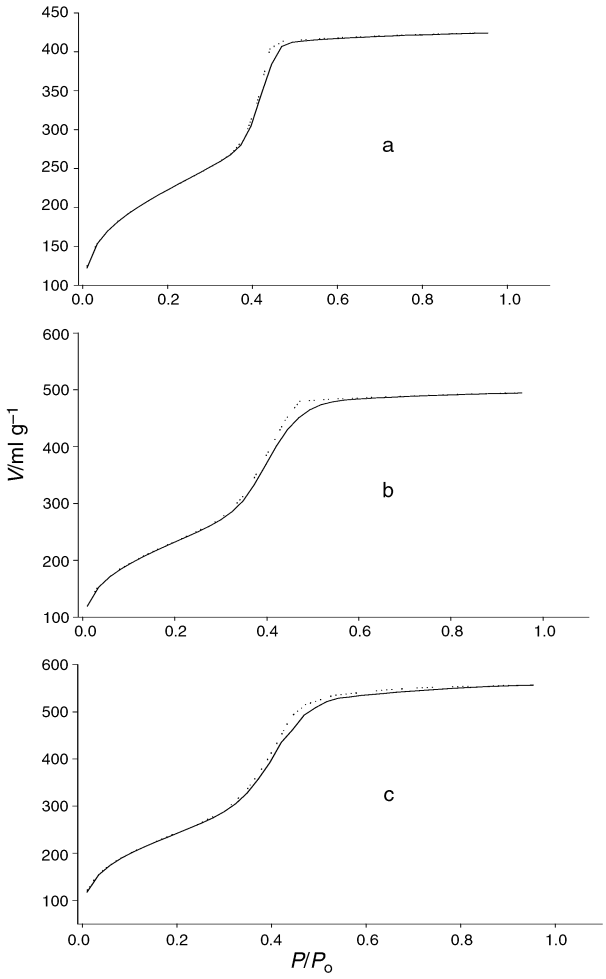

Fig. 1 Nitrogen adsorption (solid line)/desorption (dotted line) isotherms for calcined mesoporous silicate materials for (a) H_I-SiO_2, (b) L_∞-SiO_2 and (c) S-SiO_2 (relative pressure is p/p_o, where p is the equilibrium pressure of the adsorbate and p_o is the saturation pressure of the adsorbate at the temperature of the adsorbent; V is the volume adsorbed at STP).

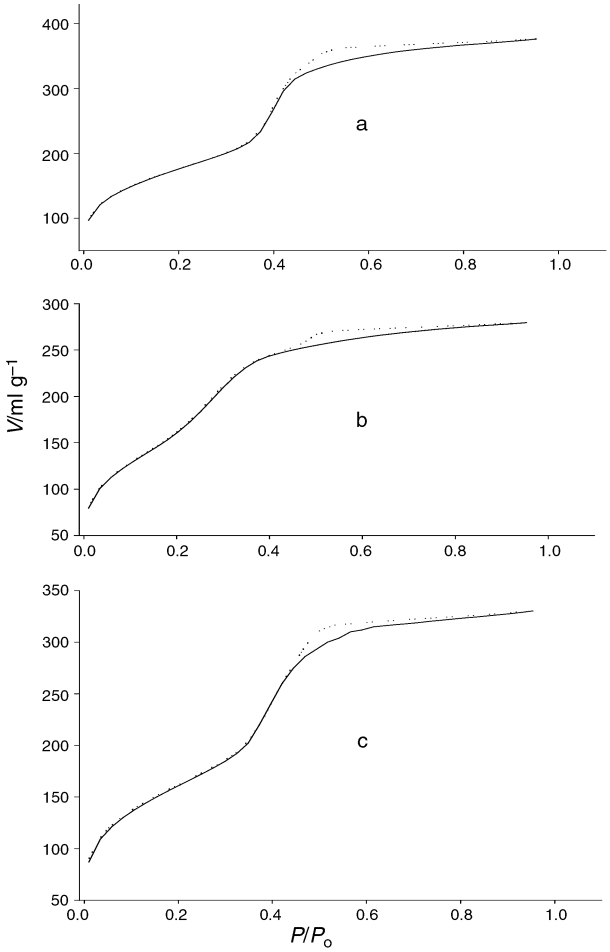

Fig. 2 Nitrogen adsorption (solid line)/desorption (dotted line) isotherms for calcined mesoporous silicate materials for (a) *Ia3d*-SiO_2, (b) *Im3m*-SiO_2 and (c) $P6_3/mmc$-SiO_2.

materials exhibited type IV isotherms, typical of mesoporous materials with pore size less than 40 Å.[24,25] A sharp inflection between relative pressure $P/P_o = 0.25$ and 0.5 indicates capillary condensation within uniform mesophases. This inflection point depends on the pore size and the sharpness in this step signifies a uniform pore size. In addition, the initial step at low relative pressure can be extrapolated to the origin, suggesting monolayer N_2 adsorption on the walls of mesopores. Hysteresis loops in the adsorption/desorption isotherms that are intermediate between type H_1-, and H_2-models are shown in Fig. 1.[26] Such a combination of H_1 and H_2 hysteresis loops can be attributed to capillary condensation associated with large pore channels.[27,28]

On the other hand, N_2 adsorption/desorption isotherms (shown in Fig. 2) show a clear type H_3 hysteresis loop at higher relative pressure. This may be attributed to N_2 filling the textural mesopores associated with slit-shaped or plate-like particles.[29]

The BET surface area and the total pore volume at relative pressure (P/P_o) = 0.953 of the calcined materials were calculated and are summarised in Table 1. It seems that the concentration of the template and the temperature during the synthesis of the mesoporous materials influence both the surface area and pore volume. The surface area of the mesoporous materials was found to be in the range 580–950 $m^2\ g^{-1}$, reflecting a high internal surface area of the mesoporous frameworks.[20,21]

The Horvath–Kawazoe (HK) pore size distribution for calcined mesoporous materials are shown in Fig. 3, and presented in Table 1. Generally, desorption data are often used for assessment of the distribution pore size curve. However, a type

Table 1 Results of the total pore volume (V) at $P/P_0 = 0.953$, surface area (A) and pore diameter (a) of the calcined mesoporous materials

Mesophase material	Template concentration(%)	T/°C	V/ $cm^3\ g^{-1}$	a/Å	A/ $m^2\ g^{-1}$
H_1-SiO_2	50	25	0.656	38	787
L_∞-SiO_2	75	25	0.765	37	852
S-SiO_2	87	25	0.861	39	950
*Ia*3*d*-SiO_2	70	60	0.582	36	624
*Im*3*m*-SiO_2	76	60	0.564	35	604
$P6_3/mmc$-SiO_2	81	60	0.511	34	580

H_3 hysteresis loop found for the high temperature synthesised mesoporous materials is unlikely to yield a reliable estimation of pore size distribution.[26] Therefore, the adsorption data was used to determine the mesopore size distribution as shown in Fig. 3(d)–(f).

Powder X-ray diffraction (XRD)

XRD was used primarily to probe the periodicity of the mesoporous materials. These types of material display a very high intensity peak around $2\theta = 2^\circ$ together with low intensity

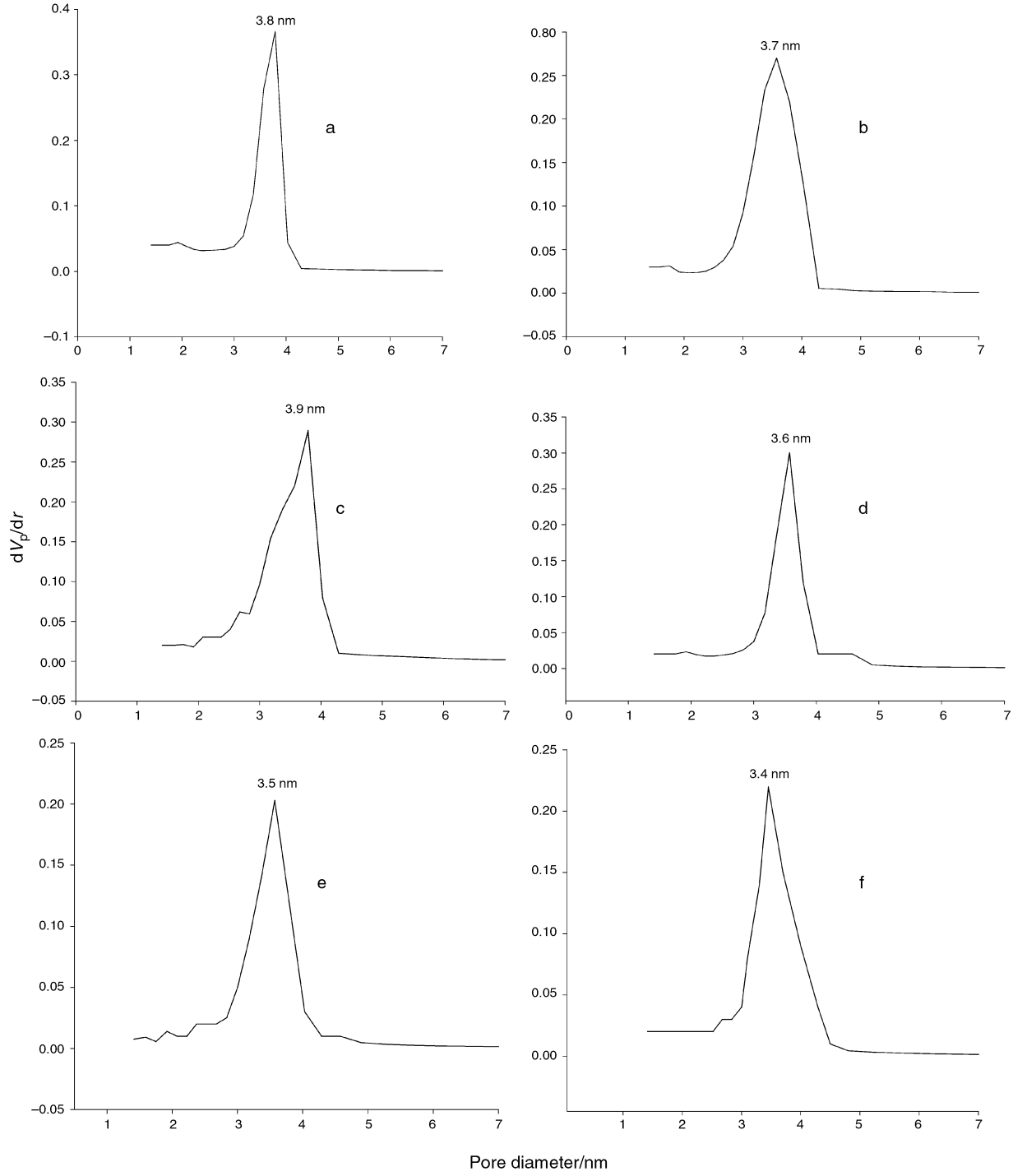

Fig. 3 Horvath–Kawazoe plots of N_2 desorption data for (a) H_1-SiO_2, (b) L_∞-SiO_2 and (c) S-SiO_2 and N_2 adsorption data for (d) *Ia*3*d*-SiO_2, (e) *Im*3*m*-SiO_2 and (f) $P6_3/mmc$-SiO_2 mesoporous materials (dV_p/dr is the derivative of the nitrogen volume adsorbed with respect to the pore diameter of the adsorbent).

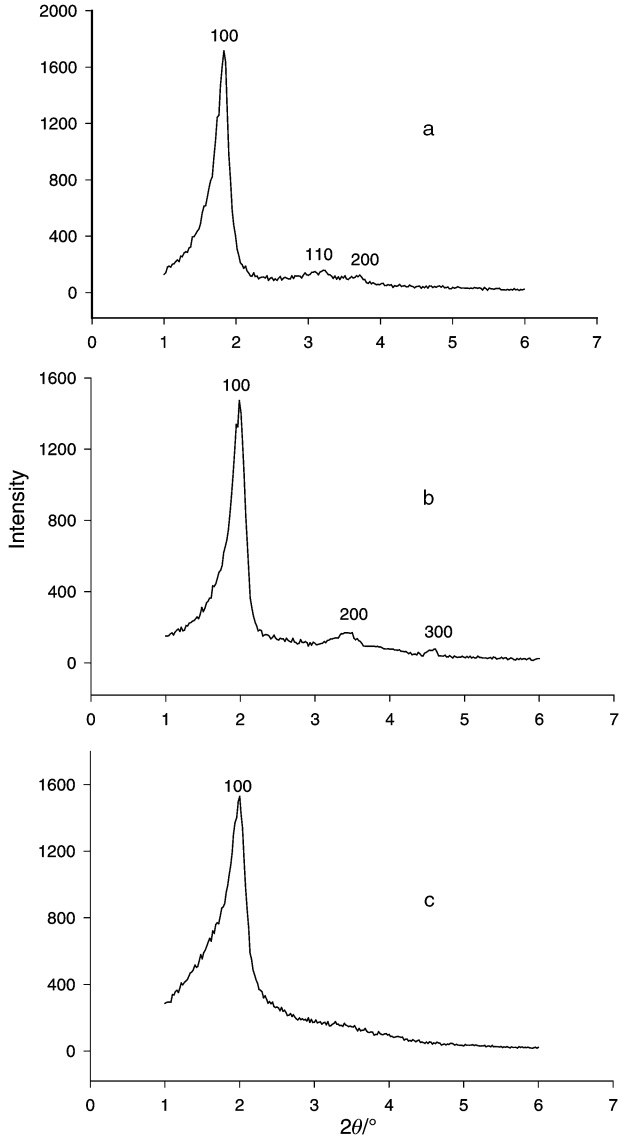

Fig. 4 XRD patterns of calcined mesoporous silicate materials synthesised at 25 °C: (a) H_I-SiO_2, (b) L_∞-SiO_2 and (c) S-SiO_2.

peaks in the 2θ range 3–8°.[1,2] Figs. 4 and 5 illustrate that the calcined samples of the lyotropic liquid crystal mesophase materials yield well-resolved XRD patterns. A long-range hexagonal order of H_I-SiO_2 was observed, as indicated by the presence of d_{100}, d_{110} and d_{200} reflections, Fig. 4(a).[30–32] The low-angle XRD pattern of H_I-SiO_2 shows a d_{100}-spacing of 48 Å, which is similar to that reported for lyotropic mesophase silicate materials.[33] The pattern shown in Fig. 4(b) can be indexed to the lamellar spacing ratios 1 : 2 : 3. The presence of these *hkl* reflections with a unit cell parameter of 44 Å for the synthesised mesoporous sample with 75% of Brij 76 at 25 °C has been established for lamellar phase materials.[34] By increasing of the template concentration to 87% (w/w) of Brij 76 (Table 1), the solid phase mesoporous material (S-SiO_2) can be characterised in accord with the Brij 76 phase diagram.[23,35] However, the XRD pattern shows a high intensity reflection peak with the same lamellar unit cell parameter = 44 Å, Fig. 4(c). This suggests that the mesoporous silica materials of the lyotropic liquid crystal solid mesophase have well-defined lamellar order. The broadening of the high intensity 100 reflection peak and the partial collapse in the low intensity d_{200} and d_{300} reflections may be ascribed to a lack of long-range crystallographic order or to finite size effects.[6,20,36]

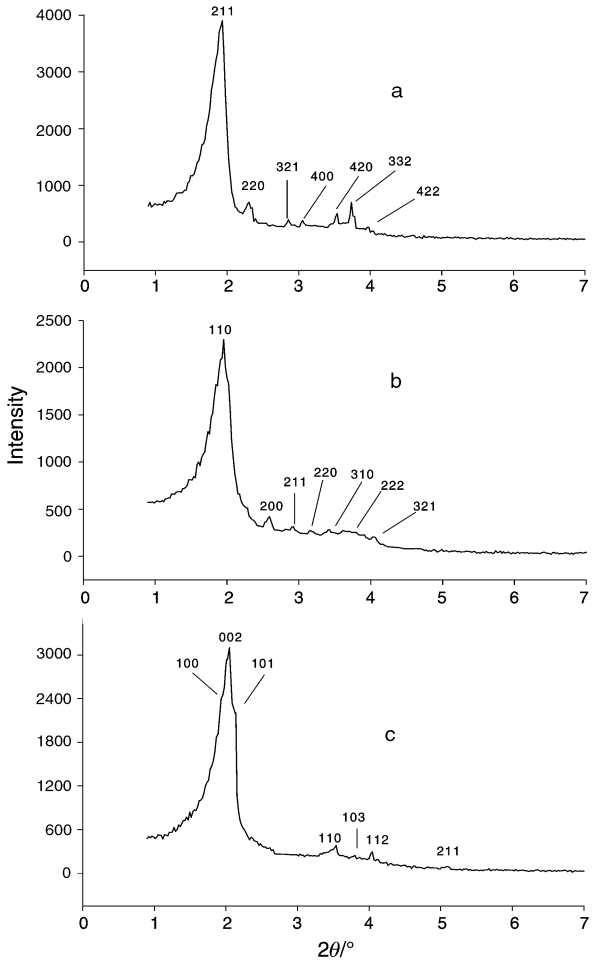

Fig. 5 XRD patterns of calcined mesoporous silicate materials synthesised at 60 °C: (a) *Ia*3*d*-SiO_2, (b) *Im*3*m*-SiO_2 and (c) $P6_3/mmc$-SiO_2.

XRD patterns of the high temperature as-synthesised materials are observed to display several distinguishable Bragg peaks which can be related to different *hkl* reflections, Fig. 5. The mesoporous silica material produced by using 70% of Brij 76 at 60 °C shows XRD reflection peaks that can be assigned to cubic lattices of space group symmetries *Ia*3*d* ($\sqrt{6} : \sqrt{8} : \sqrt{14} : \sqrt{16} : \sqrt{20} : \sqrt{22} : \sqrt{24}$), Fig. 5(a).[1,2,37] The presence of the finely resolved peaks with *d*-spacings of 46, 39.8, 30.0, 28.2, 25.2, 24.0 and 22.9 Å are similarly observed in MCM-48 mesoporous materials.[38]

The XRD pattern (Fig. 5(b)) for the calcined mesoporous material prepared at high concentration of Brij 76 (76%), exhibits well-ordered reflection peaks of the cubic *Im*3*m* space group.[27,39] These peaks display *d*-value ratios of $\sqrt{2} : \sqrt{4} : \sqrt{6} : \sqrt{8} : \sqrt{10} : \sqrt{12} : \sqrt{14}$, which are indicative of (110, 200, 211, 220, 310, 222, 321) reflections, respectively. This type of material is consistent with SBA-16 mesoporous silica material.[39] Fig. 5(c) shows the XRD patterns of the calcined mesoporous silica prepared in the presence of Brij 76 (81%) as template. Three poorly resolved peaks appear in the 2θ range 1–2° with *d*-spacings of 45.2, 43.5 and 39 Å. In addition, two resolved peaks in the 2θ range 3–5° with *d*-spacings of 25.2 and 21.3 Å are observed. These peaks correspond to the 100, 002, 101, 110 and 112 reflections, respectively. Such an XRD pattern is assigned to the three-dimensional $p6_3/mmc$ hexagonal structure with unit cell parameters of, $\psi = 55.2$, $c = 87$ Å, with $c/\psi = 1.58$ which are consistent with the synthesised three-dimensional hexagonal mesophase, SBA-2.[39,40] These results established that the three-dimensional hexagonal structure is formed from hexagonal

close packing globular aggregate structures.[41] Besides, the appearance of the low intensity 103 and 211 reflection peaks resembles that of well-defined long-range ordered mesoporous silica materials ($p6_3/mmc$-SiO_2).

In the view of the XRD patterns, it may be concluded that the use of high synthesis temperatures leads to the formation of three-dimensional, bicontinuous and cylindrical mesoporous silicate structures rather than one-dimensional mesoporous materials.[42]

Transmission electron micrographs (TEM)

TEM was used to investigate the structure of the mesophase materials, as shown in Fig. 6. The calcined samples were utilised for the TEM studies since the stability of these samples enhanced the TEM images.

The TEM image for selected particles along the [100] direction in Fig. 6(a) shows regular arrays of uniform channels in a hexagonal texture. The separation distance between the

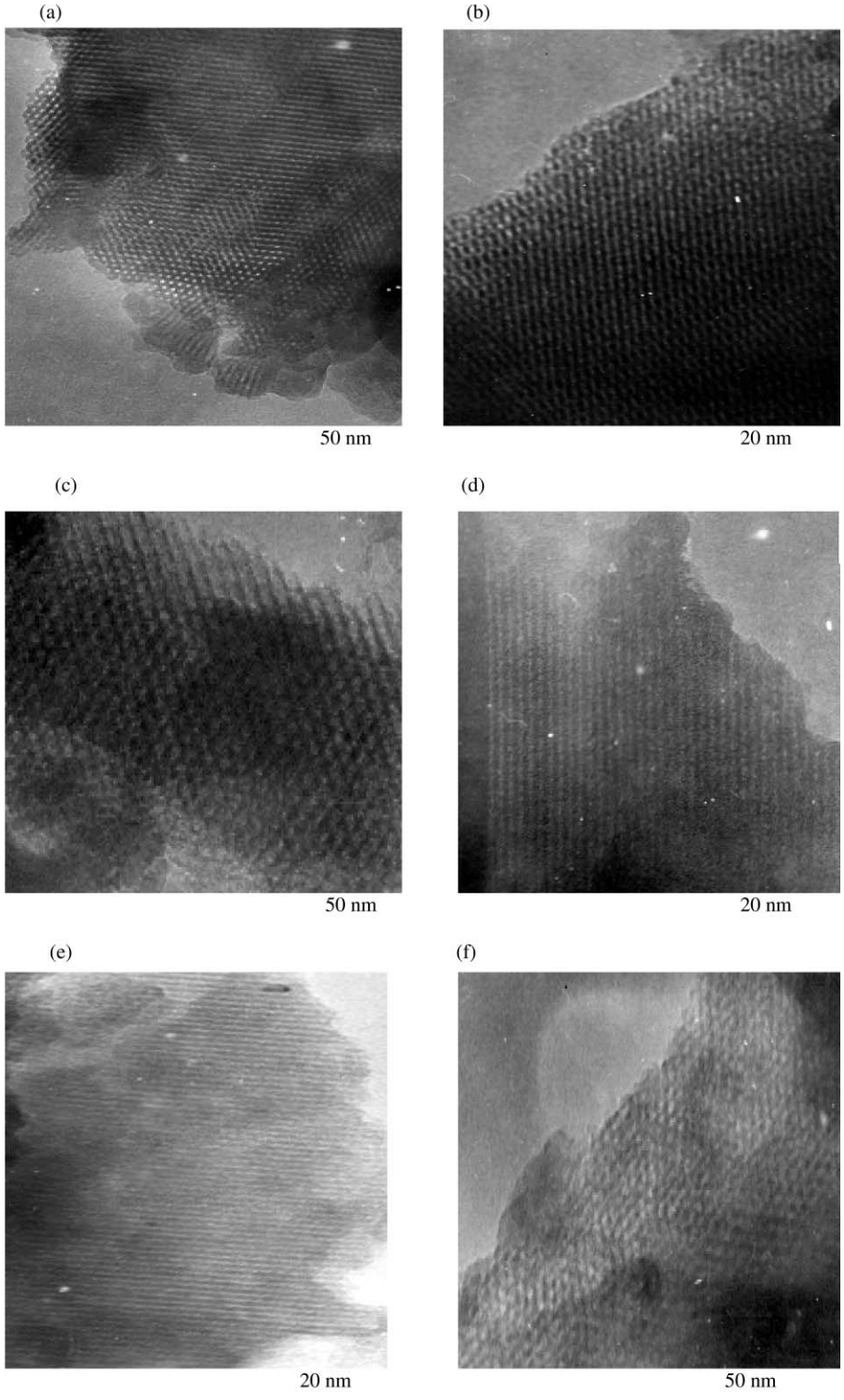

Fig. 6 TEM images of calcined mesoporous silicate materials: (a) H_1-SiO_2, (b) $Im3m$-SiO_2, (c) $Ia3d$-SiO_2, (d) L_∞-SiO_2, (e) S-SiO_2 and (f) $P6_3/mmc$-SiO_2.

channels is about 44 Å, which is consistent with the d_{100} X-ray reflection peak.[2,43] The TEM image shown in Fig. 6(b), shows the mesoporous silica material (*Im*3*m*-SiO_2). The characteristics of the TEM pattern suggests the presence of highly ordered three-dimensional cubic *Im*3*m* mesostructure.[2,39] The selected view of the [100] projection in Fig. 6(c) shows a uniform pore structure along the [100] direction. These results are consistent with the bicontinuous cubic *Ia*3*d* liquid crystal phase that has been reported previously.[1,43,44] Whilst it is difficult from one direction only of TEM images to definatively assign the three dimensional cubic *Ia*3*d* mesostructure,[45] in this case the TEM images show several distinguishable X-ray reflection peeks of the cubic silica material (*Ia*3*d*-SiO_2).[46] Fig. 6(d) and (e) shows the TEM patterns of the lamellar (L_∞) and solid phase (S) mesoporous silica materials, respectively. Both images exhibit highly ordered layers indicating the existence of a lamellar lyotropic liquid crystal phase.[47] The interlayer separation of both samples is about 40 Å, which is in good agreement with the position of the d_{100} reflection peak from X-ray analyses, Fig. 4(b) and (c).[48]

P6_3/*mmc* space symmetry and a three-dimensional hexagonal mesoporous silica structure have been confirmed for the TEM image of Fig. 6(f). However, the TEM patterns show a regular array of mesopores characteristic of the [$\bar{1}$ $\bar{1}$ 23] orientation, which is indicative of 3-d hexagonal mesophases.[39,49] In this case, well-ordered large channels are observed to be arranged in the same manner as 3-d hexagonal mesoporous silica materials of group symmetry (*P*6_3/*mmc*) that have been prepared in bulk silica mesophases.[50–52]

Conclusion

The formation of well-defined long-range ordered mesoporous silica materials has been achieved by using high concentrations of non-ionic surfactant (Brij 76) and under strongly acidic conditions. The pre-existence of the lyotropic liquid crystal mesophases directed the formation of monolithic nanostructured materials through the liquid crystal template mechanism. The monolithic family includes materials with hexagonal (H_I-SiO_2), lamellar (L_∞-SiO_2), solid phase (S-SiO_2), cubic (*Ia*3*d*-SiO_2), cubic (*Im*3*m*-SiO_2) and 3-d hexagonal (*p*6_3/*mmc*-SiO_2) structure mesophases. At high temperature (*ca.* 60 °C), the formation of three-dimensional mesoporous structures is favoured.

N_2 adsorption/desorption isotherm curves established that all the synthesised materials have uniform mesophases without any micropore architictures. These materials have BET surface areas in the range 580–950 $m^2\ g^{-1}$ and pore sizes of 34–39 Å. Such high surface areas and large pore sizes are a consequence of the relatively low synthesis temperatures. XRD and TEM analyses established reliable synthesis of these well-defined mesoporous silicates.

Acknowledgements

We thank Dr B. Cressey and C. P. Ship for their help with TEM measurements. We also appreciate Dr G. S. Attard for fruitful discussions.

References

1 C. T. Kresge, M. E. Leonowicz, W. J. Roth, J. C. Vartuli and J. S. Beck, *Nature*, 1992, **359**, 710.
2 J. S. Beck, J. C. Vartuli, W. J. Roth, M. E. Leonowicz, C. T. Kresge, K. D. Schmitt, C. T. W. Chu, D. H. Olsan, E. W. Higgins and J. L. Schlenker, *J. Am. Chem. Soc.*, 1992, **114**, 10834.
3 Q. Huo, D. I. Morgalese, U. Ciesla, P. Y. Feng, T. E. Gier, P. Sieger, R. Leon, A. Firouzi, B. F. Chmelka, F. Schuth and G. D. Stucky, *Nature*, 1994, **368**, 317.
4 Q. Huo, D. I. Morgalese, U. Ciesla, D. G. Demuth, P. Y. Feng, T. E. Gier, P. Sieger, R. Leon, P. M. Petroff, F. Schuth and G. D. Stucky, *Chem. Mater.*, 1994, **6**, 1176.
5 S. Inagaki, Y. Fukushima and K. Kuroda, *J. Chem. Soc., Chem. Commun.*, 1993, 680.
6 S. A. Bagshaw, E. Prouzet and T. J. Pinnavaia, *Science*, 1995, **269**, 1242.
7 P. T. Tanev and T. J. Pinnavaia, *Science*, 1995, **267**, 865.
8 D. Y. Zhao and D. J. Goldfarb, *J. Chem. Soc., Chem. Commun.*, 1995, 875.
9 V. Alfredsson and M. W. Anderson, *Chem. Mater.*, 1996, **8**, 1141.
10 A. A. Romero, M. D. Alba and J. Klinowski, *J. Phys. Chem. B*, 1998, **102**, 123.
11 A. A. Romero, M. D. Alba, W. Z. Zhou and J. Klinowski, *J. Phys. Chem. B*, 1997, **101**, 5294.
12 M. Kruk, M. Jaroniec, R. Ryoo and J. M. Kim, *Chem. Mater.*, 1999, **11**, 2568.
13 A. Ayyappan and C. N. R. Rao, *Chem. Commun.*, 1997, 575.
14 A. Steel, S. W. Carr and M. W. Anderson, *J. Chem. Soc., Chem. Commun.*, 1994, 1571.
15 J. Luo and S. L. Suib, *Chem. Commun.*, 1997, 1031.
16 M. Ogawa, *J. Am. Chem. Soc.*, 1994, **116**, 7941.
17 G. S. Attard, J. C. Glyde and C. G. Göltner, *Nature*, 1995, **378**, 366.
18 G. S. Attard, P. N. Bartlett, N. R. B. Coleman, J. M. Elliott, J. R. Owen and J. H. Wang, *Science*, 1997, **278**, 838.
19 G. S. Attard, M. Edgar and C. G. Göltner, *Acta Mater.*, 1998, **46**, 751.
20 J. Evans, A. B. Zaki, M. Y. El-Sheikh and S. A. El-Safty, *J. Phys. Chem. B*, 2000, **104**, 10271.
21 S. A. El-Safty, A. B. Zaki, M. Y. El-Sheikh and J. Evans, *Colloids Surf.*, 2001, in press.
22 X. S. Zhao, G. Q. Lu and G. J. Millar, *Ind. Eng. Chem. Res.*, 1996, **35**, 2075.
23 G. S. Attard, P. N. Bartlett, N. R. B. Coleman, J. M. Elliott and J. R. Owen, *Langmuir*, 1998, **14**, 7340.
24 R. Schmidt, E. W. Hansen, M. Stocker, D. Akporiaye and O. H. Ellestad, *J. Am. Chem. Soc.*, 1995, **117**, 4049.
25 P. J. Branton, P. G. Hall, K. S. W. Sing, H. Reichert, F. Schuth and K. K. Unger, *J. Chem. Soc., Faraday Trans.*, 1994, **90**, 2965.
26 S. J. Gregg and K. S. Sing, *Adsorption, Surface Area and Porosity*, 2nd edn., Academic Press, London, 1992.
27 P. Yang, D. Zhao, D. I. Margolese, B. F. Chmelka and G. D. Stucky, *Nature*, 1998, 152.
28 P. L. Llewellyn, Y. Grillet, F. Schuth, H. Reichert and K. K. Unger, *Microporous Mater.*, 1994, **3**, 345.
29 S. S. Kim, W. Zhang and T. J. Pinnavaia, *Science*, 1998, **282**, 1302.
30 D. Wei, H. Wang, X. Feng, W. Chuch, P. Ravikovitch, M. Lyubovsky, C. Li, T. Takeguchi and G. L. Haller, *J. Phys. Chem. B*, 1999, **103**, 2113.
31 A. S. Bagshaw, E. Pruzet and T. J. Pinnavaia, *Science*, 1995, **269**, 1242.
32 S. Inagaki, A. Koiwai, N. Suzuki, Y. Fukushima and K. Kuroda, *Bull. Chem. Soc. Jpn.*, 1996, **69**, 1449.
33 A. Firouzi, F. Atef, A. G. Oertli, G. D. Stucky and B. F. Chmekia, *J. Am. Chem. Soc.*, 1997, **119**, 3596.
34 Z. Luan, H. He, W. Zhou and J. Klinowski, *J. Chem. Soc., Faraday Trans.*, 1998, **94**, 979.
35 D. J. Mitchell, J. T. Tiddy, L. Waring, T. Bostock and M. P. McDonald, *J. Chem. Soc., Faraday Trans.*, 1983, **79**, 975.
36 C. Y. Chem, X. H. Li and M. E. Davis, *Microporous Mater.*, 1993, **2**, 27.
37 J. M. Kim, S. S. Kim and R. Ryoo, *Chem. Commun.*, 1998, 259.
38 J. Medina, J. A. Montoya and J. A. Reyes, *Stud. Surf. Sci. Catal.*, 1998, **118**, 889.
39 D. Zhao, Q. Huo, J. Feng, B. F. Chmelka and G. D. Stucky, *J. Am. Chem. Soc.*, 1998, **120**, 6024.
40 Q. Huo, D. I. Margolese and G. D. Stucky, *Chem. Mater.*, 1996, **8**, 1147.
41 H. Hagslatt, O. Soderman and B. Jonsson, *Langmuir*, 1994, **10**, 2177.
42 M. J. Kim and R. Ryoo, *Chem. Mater.*, 1999, **11**, 487.
43 D. Zhao and D. Goldfarb, *Stud. Surf. Sci. Catal.*, 1995, **97**, 181.
44 J. Xu, Z. Luan, H. He, W. Zhou and L. Kevan, *Chem. Mater.*, 1998, **10**, 3690.
45 V. Alfredsson, M. W. Anderson, T. Ohsuna, O. Terasaki, M. Jacob and M. Bojrup, *Chem. Mater.*, 1997, **9**, 2066.
46 F. Chen, L. Huang and Q. Li, *Chem. Mater.*, 1997, **9**, 2685.
47 M. Templin, A. Franck, A. D. Chesne, H. Leist, Y. Zhang, R. Ulrich, V. Schädler and U. Wiesner, *Science*, 1997, **278**, 1795.
48 S. Ayyappan and C. N. R. Rao, *Chem. Commun.*, 1997, 575.

49 Y. Lu, R. Ganguli, C. A. Drewien, M. T. Anderson, C. J. Brinker, W. Gong, Y. Guo, H. Soyes, B. Dunn, M. H. Huang and J. I. Zink, *Nature*, 1997, **389**, 364.
50 Q. Huo, R.. Leon, P. M. Petroff and G. D. Stucky, *Science*, 1995, **268**, 1324.
51 J. N. Israelachvili, D. J. Mitchell and B. W. Ninham, *J. Chem. Soc., Faraday Trans. 2*, 1976, **72**, 1525.
52 J. N. Israelachvili, D. J. Mitchell and B. W. Ninham, *Biochim. Biophys. Acta*, 1977, **470**, 185.